$(CO)_3Cl)_2$ attached to it. The second metal system (rhenium) perturbs the system by lowering the π^* energy levels of the bridging ligand. This lowers the energy of the ^{1}MLCT transition and the reduction potential for the $d\pi^6/d\pi^6\pi^{*1}$ couple.

Acknowledgment. We thank the Office of Energy Science of the Department of Energy for support under Grant DE-FG05-84ER-13263.

Supplementary Material Available: Table V, giving elemental analyses of some of the ruthenium(II)/rhenium(I) compounds (1 page). Ordering information is given on any current masthead page.

Contribution from the Department of Chemistry, Northern Illinois University, DeKalb, Illinois 60115

Crystal Structures and Solution Electronic Absorption and MCD Spectra for Perchlorate and Halide Salts of Binuclear Gold(I) Complexes Containing Bridging $Me_2PCH_2PMe_2$ (dmpm) or $Me_2PCH_2CH_2PMe_2$ (dmpe) Ligands

Huey-Rong C. Jaw, M. Meral Savas, Robin D. Rogers,* and W. Roy Mason*

Received August 17, 1988

Perchlorate and bromide salts of $Au_2(dmpm)_2^{2+}$ and perchlorate, chloride, bromide, and iodide salts of $Au_2(dmpe)_2^{2+}$ were crystallized and studied by X-ray diffraction. $[Au_2(dmpm)_2](ClO_4)_2$ crystallizes in the monoclinic space group $C2/m$ with a = 9.608 (5) Å, b = 13.317 (5) Å, c = 9.039 (5) Å, β = 97.50 (5)°, and D_{calcd} = 2.51 g cm^{-3} for Z = 2. The methyl group and CH_2 bridging atoms are disordered, resulting in two different chair conformations for the eight-membered cation ring. The Au···Au distance is 3.028 (2) Å. The perchlorate anions are also fractionally disordered. $[Au_2(dmpm)_2]Br_2\cdot 2H_2O$ is triclinic, $P\bar{1}$, with a = 8.005 (1) Å, b = 8.007 (3) Å, c = 10.111 (3) Å, α = 66.61 (5)°, β = 75.84 (2)°, γ = 70.70 (2)°, and D_{calcd} = 2.56 g cm^{-3} for Z = 1. The cation exists in a chair conformation with a Au···Au separation of 3.023 (1) Å. $[Au_2(dmpe)_2](ClO_4)_2\cdot H_2O$ is tetragonal, $P4_22_12$, with a = 9.486 (5) Å, c = 16.053 (3) Å, and D_{calcd} = 2.09 g cm^{-3} for Z = 2. The anion and solvent are disordered; the Au···Au distance in the cation is 2.872 (2) Å. $[Au_2(dmpe)_2]Cl_2\cdot 2H_2O$ and $[Au_2(dmpe)_2]Br_2\cdot 1.5H_2O$ are isostructural, with one anion and the water molecules disordered. The bromide analogue crystallizes with one disordered solvent site empty. Both are triclinic, $P\bar{1}$, with a = 8.661 (9) Å, b = 11.582 (6) Å, c = 13.600 (4) Å, α = 69.62 (3)°, β = 69.00 (6)°, γ = 83.87 (7)°, and D_{calcd} = 2.23 g cm^{-3} for Z = 1 (Cl) and a = 8.575 (7) Å, b = 11.841 (6) Å, c = 13.251 (9) Å, α = 71.02 (6)°, β = 71.44 (7)°, γ = 86.43 (6)°, and D_{calcd} = 2.43 g cm^{-3} for Z = 1 (Br). The Au···Au separation is 2.9265 (5) Å in the chloride and 2.9438 (5) Å in the bromide. $[Au_2(dmpe)_2]I_2\cdot CH_3CN$ is monoclinic, $P2_1/c$, with a = 10.436 (5) Å, b = 24.970 (8) Å, c = 20.383 (8) Å, β = 96.53 (4)°, and D_{calcd} = 2.49 g cm^{-3} for Z = 8. The two unique Au···Au distances average 2.974 (3) Å. Electronic absorption and magnetic circular dichroism (MCD) spectra are presented for dilute $HClO_4$ and CH_3CN solutions. The spectra of the ClO_4^- salts reveal two low-energy band systems and accompanying negative MCD B terms that are interpreted as Au_2-localized transitions $d\sigma^* \rightarrow p\sigma$. Several higher energy bands are ascribed to AuP_2-localized transitions. The spectra of the halide salts in CH_3CN do not obey Beer's law, and their concentration dependence is attributed to halide association to form $Au_2P_4X^+$ species. Association constants are determined from quantitative dependence of the spectra on cation and halide concentrations. The spectral transitions for the $Au_2P_4X^+$ species are assigned as $X^- \rightarrow Au_2^{2+}$ ligand to metal charge transfer (LMCT). The importance of Au-Au interaction in the annular complexes in the solid and in solution is discussed.

Introduction

Gold(I) forms an interesting class of binuclear complexes with certain bidentate ligands.[1-10] The structures of these complexes consist of eight-membered rings **1** in which two nearly linear two-coordinate AuX_2 units are linked together and feature a relatively short trans annular Au-Au distance. Typical values of the Au-Au distance include 2.76 (1) Å in $[Au_2(S_2CN(Pr^n)_2)_2]$,[6] 2.876 Å in $[Au_2((CH(Ph_3P))_2CO)_2]$,[10] 2.888 (3) Å in $[Au_2((Ph_2P)_2CH)_2]$,[1] 3.010 (1) Å in $[Au_2((Me_2P)_2CH_2)_2]Cl_2\cdot 2H_2O$,[4] 3.023 Å in $[Au_2((CH_2)_2PEt_2)_2]$,[9] and ~3.04 Å in $[Au_2(S_2P(OPr^i)_2)_2]$[7] (for comparison, the interatomic distance in Au metal, 2.884 Å,[11] lies within this range of Au-Au distances). The Au(I) centers in these complexes have closed-shell $5d^{10}$ electron configurations and are therefore formally nonbonded. However, at the observed distances (0.4-0.6 Å less than van der Waals contacts of 3.4 Å[12]) there is clearly significant intramolecular Au-Au interaction. The detailed nature and electronic structural consequences of this interaction are not well understood. Most of

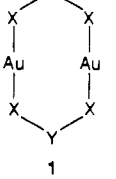

1

X = PPh_2; Y = CH,[1] CH_2,[2] NH[3]
X = PMe_2; Y = CH_2,[4] $(CH_2)_2$,[5] $(CH_2)_3$[5]
X = S; Y = CNR_2,[6] $P(OR)_2$,[7] COR[8]
X = CH_2; Y = PR_2[9]
X = $CH(PPh_3)$; Y = CO[10]

(1) Briant, C. E.; Hall, K. P. Mingos, D. M. P. *J. Organomet. Chem.* **1982**, *229*, C5. Schmidbauer, H.; Mandl, J. R.; Bassett, J.-M.; Blaschke, G.; Zimmer-Gasser, B. *Chem. Ber.* **1981**, *114*, 433.
(2) Schmidbauer, H.; Wohlleben, U. S.; Frank, A.; Huttner, G. *Chem. Ber.* **1977**, *110*, 2751.
(3) Uson, R.; Laguna, A.; Laguna, M.; Fraile, M. N.; Jones, P. G.; Sheldrick, G. M. *J. Chem. Soc., Dalton Trans.* **1986**, 291.
(4) Kozelka, J.; Oswald, H. R.; Dubler, E. *Acta Crystallogr.* **1986**, *C42*, 1007.
(5) Ludwig, W.; Meyer, W. *Helv. Chim. Acta* **1982**, *65*, 934.
(6) (a) Hesse, R.; Jennische, P. *Acta Chem. Scand.* **1972**, *26*, 3855. (b) Åkerstrom, S. *Ark. Kemi* **1959**, *14*, 387. (c) Farrell, F. J.; Spiro, T. G. *Inorg. Chem.* **1971**, *10*, 1606. (d) Miller, J. B.; Burmeister, J. L. *Synth. React. Inorg. Met.-Org. Chem.* **1985**, *15*, 223.
(7) Lawton, S. L.; Rohrbaugh, W. J.; Kokotailo, G. T. *Inorg. Chem.* **1972**, *11*, 2227.
(8) Weinstock, J.; Sutton, B. M.; Kuo, G. Y.; Walz, D. T.; DiMartino, M. J. *J. Med. Chem.* **1974**, *17*, 139.
(9) Schmidbauer, H.; Mandl, J. R.; Richter, W.; Bejenke, V.; Frank, A.; Huttner, G. *Chem. Ber.* **1977**, *110*, 2236.
(10) Vicente, J.; Chicote, M.-T.; Sauva-Llamas, I.; Jones, P. G.; Meyer-Bäse, K.; Erdbrügger, C. F. *Organometallics* **1988**, *7*, 997.
(11) Sutton, L. E., Ed. *Chemical Society Special Publication 11*; Chemical Society: London, 1958; p 53.
(12) Bondi, A. *J. Phys. Chem.* **1964**, *68*, 441.

0020-1669/89/1328-1028$01.50/0

the studies of complexes **1** have been concerned with synthesis and structure determination. However, recently the Au–Au interaction has been examined from an extended Hückel MO viewpoint,[13] which suggested that mixing of the 6s, $6p_z$, and $5d_{z^2}$ orbitals (Au–Au vector along the z axis) of the two Au atoms results in a bonding interaction. Also, some electronic absorption spectra have been reported[5] for several binuclear complexes containing different bidentate phosphines and a bidentate ylid ligand. The lowest energy bands in the UV region were found at lower energy than those of related mononuclear Au(I) complexes. Localized Au_2 transitions were suggested for these bands, but few details were given.

In order to further characterize the electronic structure of complexes of type **1** and to provide additional experimental information concerning the details of the Au–Au interaction, a systematic structural and spectroscopic study of representative examples has been undertaken. This paper reports crystal structures for $[Au_2(dmpm)_2](ClO_4)_2$, $[Au_2(dmpm)_2]Br_2\cdot 2H_2O$ (dmpm = bis(dimethylphosphino)methane), $[Au_2(dmpe)_2](ClO_4)_2\cdot H_2O$, $[Au_2(dmpe)_2]Cl_2\cdot 2H_2O$, $[Au_2(dmpe)_2]Br_2\cdot 1.5H_2O$, and $[Au_2(dmpe)_2]I_2\cdot CH_3CN$ (dmpe = bis(dimethylphosphino)ethane). The crystal structure for $[Au_2(dmpm)_2]Cl_2\cdot 2H_2O$ was reported recently by Kozelka et al.[4] and is relevant to the structures described in this paper. Solution electronic absorption and magnetic circular dichroism (MCD)[14] spectra for these compounds at room temperature in H_2O or CH_3CN are also reported and interpreted.

Experimental Section

Preparation of Compounds. The starting materials for the synthesis of the binuclear Au(I) complexes were tetra-*n*-butylammonium dibromoaurate(I), $[TBA][AuBr_2]$,[15] bis(acetonitrile)gold(I) perchlorate, $[Au(CH_3CN)_2]ClO_4$,[16] or chloro(triethylphosphine)gold(I), $Au(PEt_3)Cl$[17] (also purchased from AESAR/Johnson-Matthey). The ligands dmpm and dmpe were purchased (Strem Chemicals) and were used without further purification.

$[Au_2(dmpm)_2](ClO_4)_2$ and $[Au_2(dmpm)_2]Br_2\cdot 2H_2O$. The perchlorate salt was prepared by two separate methods. The first method involved combining dry acetone solutions of the dmpm ligand and $[TBA][AuBr_2]$ in an inert atmosphere. A yellow precipitate of $[Au_2(dmpm)_3]Br_2$[18] was formed immediately. This precipitate was collected by filtration and then dissolved in H_2O. Upon the addition of dilute (0.10 M) $HClO_4$, colorless crystals of $[Au_2(dmpm)_2](ClO_4)_2$ formed immediately. The second method of preparation was accomplished by adding a stoichiometric amount of the dmpm ligand to a CH_3CN solution of $[Au(CH_3CN)_2]ClO_4$ under an inert atmosphere. Colorless crystals formed immediately. Single crystals of $[Au_2(dmpm)_2](ClO_4)_2$ for X-ray structure determination were grown by slow evaporation of a 0.033 M $HClO_4$ solution of the salt. The crystals are air stable and exhibit a purple emission at room temperature under UV light. *Caution: perchlorate hazard!*

When the yellow $[Au_2(dmpm)_3]Br_2$ of the first method above is dissolved in H_2O, the odor of the dmpm ligand can be detected above the solution. When this solution is evaporated slowly, colorless crystals of $[Au_2(dmpm)_2]Br_2\cdot 2H_2O$ are deposited. A clear single crystal was used for X-ray structure determination, but the hydrated salt tended to lose water on standing in dry air and the clear crystals turned opaque after several days. The solid bromide salt also exhibited purple emission under UV light.

$[Au_2(dmpe)_2]Br_2\cdot 1.5H_2O$ and $[Au_2(dmpe)_2](ClO_4)_2\cdot H_2O$. The bromide salt was prepared by dropwise addition of the dmpe ligand to a stirred solution of $[TBA][AuBr_2]$ in dry acetone under an inert atmosphere. The white air-stable precipitate that was formed immediately was collected by filtration and recrystallized from undried acetone by open evaporation. This recrystallization produced single crystals of the hydrated salt suitable for X-ray diffraction. The perchlorate salt was prepared by treating an aqueous solution of the bromide salt with 1 M $HClO_4$, which resulted in a nearly quantitative yield. Single crystals were obtained by slow evaporation of a 40% aqueous CH_3CN solution. *Caution: perchlorate hazard!* Both the hydrated bromide and perchlorate salts lose water on standing in dry air, and their crystals turn opaque after several days. Both solids exhibit a bright blue emission under UV light.

$[Au_2(dmpe)_2]Cl_2\cdot 2H_2O$. The dmpe ligand was added slowly to a solution of $Au(PEt_3)Cl$ in dry acetone and stirred for 2 h under an inert atmosphere. Upon the addition of ethyl ether, a white solid precipitated and was removed. The filtrate was evaporated to dryness, and the solid residue was washed with acetone and ether and air-dried. Single crystals for X-ray were grown by slow evaporation from undried CH_3CN. Clear crystals of the hydrated salt lose water on standing in dry air and turn opaque. The solid chloride salt also exhibited a bright blue emission under UV light.

$[Au_2(dmpe)_2]I_2\cdot CH_3CN$. The starting material for the iodide salt was $Au(PEt_3)I$, which was prepared by treating $Au(PEt_3)Cl$ with [TBA]I in ethanol solution. Water was added to precipitate the white $Au(PEt_3)I$ complex. A less than stoichiometric amount of the dmpe ligand (0.50 mmol) in absolute ethanol was added to an absolute ethanol solution of $Au(PEt_3)I$ (0.76 mmol) under an inert atmosphere. A pale yellow solid was formed and was stirred for 2 h before collection by filtration. Yellow-green single crystals were grown by slow evaporation from CH_3CN. They exhibit a bright green emission under UV light but rapidly lose CH_3CN and turn dark on standing in air. The crystal for X-ray structure determination was removed from saturated CH_3CN solution, mounted, and quickly cooled to −150 °C in a stream of cold N_2 gas to prevent solvent loss.

All of the gold complexes prepared gave satisfactory elemental analysis.

X-ray Data Collection, Structure Determination, and Refinement. Single crystals of the title complexes were mounted on pins and transferred to the goniometer. The two compounds studied at low temperature were cooled to −150 °C by using a stream of cold nitrogen gas. Data were collected on an Enraf-Nonius CAD4 diffractometer using the θ–2θ scan technique. The SHELX76[19] computer programs were used in the solution and refinement of the structures. Neutral-atom scattering factors were from ref 20. A summary of the data collection and structure refinement parameters is given in Table I. Special circumstances regarding the individual determinations are described below. The final fractional coordinates are given in Table II.

$[Au_2(dmpm)_2](ClO_4)_2$. Statistical tests indicated that the space group was centric, $C2/m$ (No. 12); however, only the Au and P atoms are ordered in this space group. Nonetheless, an investigation of the acentric $C2$ (No. 5) and Cm (No. 8) revealed the continued presence of the disorder and high correlations between the Au and P positions related by the 2-fold axis and mirror plane the cation resides on in $C2/m$. Collection of data at −150 °C (reported here) did not improve the situation, and the centric $C2/m$ was chosen.

In the disorder model, all three unique carbon atoms are disordered, resulting in two chair conformations of the cations (50% occupancy each) that differ by a rotation of 180° about an axis lying equal distance between the two sets of P–Au–P axes. The perchlorate anion is also disordered. This manifests itself not just as a disorder of the oxygen atoms but as fractional disorder of the entire molecule. The anions present two different faces toward the cations: three of the four oxygen atoms arranged facing the cation versus only two. The former requires closer approach of the Cl atom and hence the fractional disorder. Each model was refined in alternate cycles at 50% occupancy each. Only the Au, P, and Cl atoms were refined anisotropically, and H atoms were not included.

$[Au_2(dmpe)_2](ClO_4)_2\cdot H_2O$. Although the cation was easily located and refined, the perchlorate anion and solvent water molecule were obviously disordered. The disorder of perchlorate ions is common; however, it was not possible to resolve the disorder and rather large isotropic thermal parameters are noted for the oxygen atoms. Complicating the disorder is an apparent fractional disorder of the chlorine atom about a 2-fold axis, as evidenced by the preferential displacement of the anisotropic thermal parameters for this atom. The acentric space group $P4_22_12$ was uniquely determined from the systematic absences. Only the Au, P, Cl, and C atoms were refined anisotropically, and the hydrogen atoms were not included.

$[Au_2(dmpe)_2]X_2\cdot nH_2O$ (X = Cl, n = 2; X = Br, n = 1.5). Two of the halide positions reside on centers of inversion in the space group $P\bar{1}$. X(2) which has its two closest contacts with Au(2) is ordered. X(3) and the

(13) Jiang, Y.; Alvarez, S.; Hoffmann, R. *Inorg. Chem.* **1985**, *24*, 749.
(14) For a review of MCD spectroscopy, together with the standard (Stephens) definitions and conventions followed here, see: Piepho, S. B.; Schatz, P. N. *Group Theory and Spectroscopy with Applications to Magnetic Circular Dichroism*; Wiley-Interscience: New York, 1983.
(15) Braunstein, P.; Clark, R. J. H. *J. Chem. Soc., Dalton Trans.* **1973**, 1845.
(16) Bravo, O.; Iwamato, R. T. *Inorg. Chim. Acta* **1969**, *3*, 663.
(17) Mann, F. G.; Wells, A. F.; Purdie, D. *J. Chem. Soc.* **1937**, 1828.
(18) Bensch, W.; Prelati, M.; Ludwig, W. *J. Chem. Soc., Chem. Commun.* **1986**, 1762.
(19) Sheldrick, G. M. "SHELX76, A System of Computer Programs for X-ray Structure Determination As Locally Modified"; University of Cambridge, 1976.
(20) *International Tables for X-ray Crystallography*; Kynoch: Birmingham, England, 1972; Vol. IV.

Table I. Crystallographic Data

chem formula	$[Au_2(dmpm)_2](ClO_4)_2$	$[Au_2(dmpm)_2]Br_2 \cdot 2H_2O$	$[Au_2(dmpe)_2](ClO_4)_2 \cdot H_2O$	$[Au_2(dmpe)_2]Cl_2 \cdot 2H_2O$	$[Au_2(dmpe)_2]Br_2 \cdot 1.5H_2O$	$[Au_2(dmpe)_2]I_2 \cdot CH_3CN$
a, Å	9.608 (5)	8.005 (1)	9.486 (5)	8.661 (9)	8.575 (7)	10.436 (5)
b, Å	13.317 (5)	8.007 (3)		11.582 (6)	11.841 (6)	24.970 (8)
c, Å	9.039 (5)	10.111 (3)	16.053 (3)	13.600 (4)	13.251 (9)	20.383 (8)
α, deg		66.61 (5)		69.62 (3)	71.02 (6)	
β, deg	97.50 (5)	75.84 (2)		69.00 (6)	71.44 (7)	96.53 (4)
γ, deg		70.70 (2)		83.87 (7)	86.43 (6)	
V, Å^3	1147	556.5	1445	1194	1205	5277.1
Z	2	1	2	1	1	8
fw	865.1	856.0	911.1	1602	1762	989.1
space group	$C2/m$ (No. 12)	$P\bar{1}$ (No. 2)	$P4_22_12$ (No. 94)	$P\bar{1}$	$P\bar{1}$	$P2_1/c$ (No. 14)
T, °C	−150	20	20	20	20	−150
λ, Å	0.71073	0.71073	0.71073	0.71073	0.71073	0.71073
ρ_{calcd}, g cm^{-3}	2.51	2.56	2.09	2.23	2.43	2.49
μ, cm^{-1}	137	176	101	123	152	131
range of rel transmission factors (corrected), %	87/100	75/100	83/100	29/100	47/100	78/100
$R(F_o)$	0.072	0.045	0.040	0.041	0.032	0.038
$R_w(F_o)$	0.082	0.046	0.044	0.046	0.033	0.043

water molecules hydrogen bonded to this halide are disordered. The halide ion is fractionally disordered across the center of inversion, and there are two unique water molecule positions resulting in four possible O···X(3) hydrogen bonds. The water molecules also hydrogen bond to X(1). An examination of the O positions revealed a difference in the number of positions occupied for the Cl^- versus Br^- salts. O(1) was present at 100% occupancy for Br^-, but O(2) was clearly at 50% occupancy. This model is also supported by the O···Br(3) and O···Br(1) contact geometries. The Cl^- salt was more complex. Each of the two unique O positions was found to exhibit fractional disorder, 2-fold disorder for O(1) (refined at 50% occupancy each) and 4-fold disorder for O(2) (refined at 25% occupancy each). It was also evident that each of the four positions around Cl(3) was occupied.

In addition to the differences observed for the water molecules, Cl(1) exhibits high thermal motion not observed for the corresponding bromide position. In the Cl^- salt the disordered oxygen atoms were refined isotropically only. Very high correlations prevented the utilization of the acentric space group, $P1$.

$[Au_2(dmpe)_2]I_2 \cdot CH_3CN$. Data for this compound were collected at −150 °C to prevent decomposition (a result of solvent loss). The number of data observed dropped off dramatically at higher θ values, and data were therefore collected up to $2\theta \leq 42°$. Of the 6206 reflections measured, only 4730 met the criteria for an observed reflection ($F_o \geq 5\sigma(F_o)$). Although more than enough data were collected to confirm the structure and study the important Au···Au parameters, it was not felt that a sufficient data to parameter ratio was available to refine all of the C and N atoms anisotropically. Anisotropic refinement was limited to the Au, I, and P atoms.

Spectral Measurements. Absorption spectra were obtained by using a Cary 1501 spectrophotometer. Absorption and MCD spectra were determined simultaneously and synchronously along the same light path by means of a computer-controlled spectrometer described elsewhere.[21] Magnetic field strength of 7.0 T was provided by a superconducting magnet system (Oxford Instruments SM2-7, equipped with a room-temperature bore tube). Solutions for absorption and MCD spectra were prepared by using dilute (0.03–0.10 M) $HClO_4$ or spectral grade CH_3CN. All spectra were corrected for the solvent blank. Solutions of the perchlorate salts in both dilute $HClO_4$ and CH_3CN obeyed Beer's law to within experimental error; however, solutions of the halide salts in acetonitrile did not. The departure from Beer's law for the halide salts was traced to an association equilibrium eq 1 (the dmpm or dmpe ligands

$$Au_2^{2+} + X^- \rightleftharpoons^{K} Au_2X^+ \qquad (1)$$

omitted for clarity). Estimates of the equilibrium association constants K were made by measuring spectra as a function of Au_2^{2+} and X^- concentration. Values of K were determined from eq 2, where $[Au_2^{2+}]_0$ and

$$K = \frac{x}{([Au_2^{2+}]_0 - x)([X^-]_0 - x)} \qquad (2)$$

$[X^-]_0$ are the initial unassociated gold complex and halide concentrations and $x = (A_{\bar{\nu}} - \epsilon_{\bar{\nu}}(Au_2^{2+})[Au_2^{2+}]_0)/(\epsilon_{\bar{\nu}}(Au_2X^+) - \epsilon_{\bar{\nu}}(Au_2^{2+}))$ with $A_{\bar{\nu}}$ = the measured absorbance at $\bar{\nu}$ and $\epsilon_{\bar{\nu}}(i)$ = the molar absorptivity of Au_2^{2+} or Au_2X^+ at $\bar{\nu}$. The derivation of eq 2 assumes a 1.00-cm path, and $\bar{\nu}$ is selected so that a large enough absorbance change occurs to be significant. Isosbestic points were observed for Au_2^{2+} and Au_2X^+ (dmpm and Cl^- at 3.49 and 3.86 μm^{-1}; dmpm and Br^- at 3.47 and 3.79 μm^{-1}; dmpe and Cl^- at 3.42 and 3.86 μm^{-1}; dmpe and Br^- at 3.40 and 3.79 μm^{-1}). For $Au_2(dmpe)_2^{2+}$ and $Au_2(dmpe)_2I^+$ isosbestic points were not observed when $[I^-]_0$ was larger than $[Au_2^{2+}]_0$ and self consistent values of K were found only for $[I^-]_0/[Au_2^{2+}]_0 < 0.7$. Complications due to absorption by the I^- ion in the same UV region as the complex also tended to lower the data precision. A similar loss of self-consistency in the values of K was found for $Au_2(dmpm)_2^{2+}$ and Br^- at $[Br^-]_0/[Au_2^{2+}]_0 > 1.1$, but isosbestic behavior for $Au_2(dmpm)_2^{2+}$ and $Au_2(dmpm)_2Br^+$ was clearly observed at lower ratios. In these two cases the values of K were the largest and the possibility of additional association equilibria complicating the measurements at high $[X^-]_0/[Au_2^{2+}]$ is the greatest. Measurements under these latter conditions were not pursued.

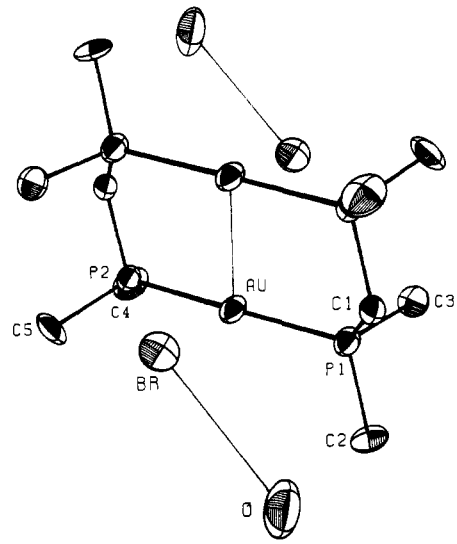

Figure 1. ORTEP illustration of $[Au_2(dmpm)_2]Br_2 \cdot 2H_2O$. The atoms are represented by their 50% probability thermal ellipsoids. Each bromide ion accepts two hydrogen bonds; the second to each bromide depicted is related to the one shown by a center of inversion.

Results and Discussion

Structures of the $[Au_2(dmpm)_2]^{2+}$ Salts. The cations found in the structures of both the perchlorate salt and the bromide dihydrate are essentially identical: a chair conformation with the two gold and four phosphorous atoms in a plane. The most accurately determined of these, $[Au_2(dmpm)_2]Br_2 \cdot 2H_2O$, is depicted in Figure 1. (The cation in the perchlorate salt was disordered such that two opposite chair conformations appear superimposed upon one another.) The contacts for both determinations are similar with Au···Au and Au–P distances of 3.028 (2) and 2.313 (5) Å, respectively, for the perchlorate salt and 3.023

(21) Mason, W. R. *Anal. Chem.* **1982**, *54*, 646.

Table II. Final Fractional Coordinates for the Gold Complexes

atom	x/a	y/b	z/c	B(eqv)[a]	atom	x/a	y/b	z/c	B(eqv)[a]
				$[Au_2(dmpm)_2](ClO_4)_2$					
Au	0.5000	0.61368 (9)	1.0000	0.80	O(2)′	0.339 (6)	0.5000	0.310 (7)	iso
P	0.3254 (5)	0.6167 (5)	0.7980 (7)	1.14	O(3)′	0.121 (4)	0.585 (3)	0.366 (4)	iso
Cl	0.224 (2)	0.5000	0.227 (2)	1.36	C(1)	0.236 (5)	0.5000	0.787 (6)	iso
Cl′[b]	0.168 (2)	0.5000	0.293 (2)	1.53	C(2)	0.188 (3)	0.714 (3)	0.816 (4)	iso
O(1)	0.364 (9)	0.5000	0.27 (1)	iso	C(3)	0.385 (4)	0.637 (3)	0.619 (4)	iso
O(2)	0.144 (4)	0.5000	0.349 (5)	iso	C(1)′	0.310 (6)	0.5000	0.702 (6)	iso
O(3)	0.195 (4)	0.584 (3)	0.135 (4)	iso	C(2)′	0.153 (4)	0.656 (4)	0.848 (5)	iso
O(1)′	0.112 (7)	0.5000	0.146 (8)	iso	C(3)′	0.365 (4)	0.704 (3)	0.652 (4)	iso
				$[Au_2(dmpm)_2]Br_2 \cdot 2H_2O$					
Au	0.90274 (8)	0.37746 (8)	0.48418 (7)	1.97	C(1)	1.108 (2)	0.197 (2)	0.794 (2)	1.73
Br	0.6917 (2)	0.6039 (3)	0.7420 (2)	3.24	C(2)	0.912 (2)	−0.041 (2)	0.794 (2)	2.98
P(1)	1.0414 (5)	0.1236 (5)	0.6671 (4)	1.81	C(3)	1.247 (2)	−0.025 (2)	0.599 (2)	2.33
P(2)	0.7711 (5)	0.6209 (5)	0.2928 (4)	1.73	C(4)	0.773 (2)	0.553 (2)	0.140 (2)	3.22
O	0.641 (2)	0.220 (2)	1.028 (2)	4.48	C(5)	0.540 (2)	0.744 (2)	0.338 (2)	3.01
				$[Au_2(dmpe)_2](ClO_4)_2 \cdot H_2O$					
Au	−0.10703 (6)	−0.10703 (6)	−1.0000	2.31	O(1)	−0.423 (6)	−0.117 (6)	−0.847 (4)	iso
P(1)	−0.0421 (5)	−0.1878 (5)	−0.8715 (3)	2.62	O(2)	−0.622 (3)	0.016 (4)	−0.854 (2)	iso
C(1)	0.135 (2)	−0.264 (2)	−0.869 (1)	3.90	O(3)	−0.501 (6)	−0.046 (4)	−0.977 (2)	iso
C(2)	−0.154 (2)	−0.328 (2)	−0.837 (1)	4.94	O(4)	−0.424 (7)	0.139 (7)	−0.917 (4)	iso
C(3)	−0.062 (2)	−0.059 (2)	−0.7866 (7)	2.68	O(5)	0.0000	−1.0000	−0.544 (2)	iso
Cl	−0.5000	0.0000	−0.8963 (5)	6.58					
				$[Au_2(dmpe)_2]Cl_2 \cdot 2H_2O$					
Au(1)	0.83526 (6)	0.39356 (4)	0.72362 (4)	1.87	C(6)	1.169 (2)	0.152 (1)	0.665 (1)	3.09
Au(2)	0.79020 (5)	0.13245 (4)	0.85999 (4)	1.79	C(7)	1.103 (2)	0.352 (1)	0.876 (1)	3.55
Cl(1)	0.5373 (8)	0.5558 (5)	0.7652 (4)	7.69	C(8)	0.973 (2)	0.594 (1)	0.810 (1)	3.23
Cl(2)	1.0000	0.0000	1.0000	4.10	C(9)	0.758 (2)	0.403 (1)	0.986 (1)	2.69
Cl(3)	0.552 (1)	1.0148 (9)	0.5198 (9)	5.65	C(10)	0.715 (2)	0.270 (1)	1.0589 (9)	2.54
P(1)	0.7590 (4)	0.3533 (3)	0.5936 (2)	1.81	C(11)	0.424 (2)	0.252 (1)	1.007 (1)	4.30
P(2)	0.9689 (4)	0.0841 (3)	0.7083 (3)	2.03	C(12)	0.557 (2)	0.040 (1)	1.136 (1)	2.98
P(3)	0.9205 (4)	0.4343 (3)	0.8492 (3)	2.20	O(11)[c]	0.6891	0.8614	0.6313	iso
P(4)	0.6170 (4)	0.1771 (3)	1.0145 (2)	2.02	O(12)	0.7087	0.7945	0.6743	iso
C(1)	0.557 (1)	0.276 (1)	0.651 (1)	2.70	O(21)	0.3609	0.7713	0.5973	iso
C(2)	0.739 (2)	0.491 (1)	0.482 (1)	2.51	O(22)	0.3312	0.7367	0.6341	iso
C(3)	0.899 (1)	0.263 (1)	0.5191 (9)	2.30	O(23)	0.3543	0.6977	0.6280	iso
C(4)	0.917 (2)	0.125 (1)	0.5820 (9)	2.62	O(24)	0.4104	0.7169	0.5846	iso
C(5)	1.000 (2)	−0.080 (1)	0.740 (1)	3.60					
				$[Au_2(dmpe)_2]Br_2 \cdot 1.5H_2O$					
Au(1)	0.81958 (5)	0.38729 (3)	0.71937 (3)	2.06	C(4)	0.903 (1)	0.1227 (9)	0.5785 (8)	2.65
Au(2)	0.77831 (4)	0.13427 (3)	0.86054 (3)	1.94	C(5)	0.987 (2)	−0.0744 (9)	0.740 (1)	3.94
Br(1)	0.5073 (2)	0.5375 (1)	0.7502 (1)	4.31	C(6)	1.157 (1)	0.160 (1)	0.6655 (9)	3.04
Br(2)	1.0000	0.0000	1.0000	4.03	C(7)	1.080 (1)	0.357 (1)	0.880 (1)	3.64
Br(3)	0.5398 (6)	1.0124 (7)	0.5011 (7)	5.70	C(8)	0.956 (1)	0.591 (1)	0.809 (1)	3.71
P(1)	0.7519 (3)	0.3439 (2)	0.5817 (2)	2.00	C(9)	0.742 (1)	0.4071 (9)	0.9812 (8)	3.45
P(2)	0.9554 (3)	0.0879 (2)	0.7082 (2)	2.13	C(10)	0.701 (1)	0.2791 (9)	1.0590 (9)	3.21
P(3)	0.9031 (3)	0.4340 (2)	0.8492 (2)	2.34	C(11)	0.407 (1)	0.236 (1)	1.007 (1)	4.52
P(4)	0.6065 (3)	0.1768 (2)	1.0152 (2)	2.29	C(12)	0.554 (1)	0.0450 (9)	1.1422 (9)	2.99
C(1)	0.548 (1)	0.2697 (9)	0.6317 (9)	2.81	O(1)[c]	0.296 (1)	1.1928 (9)	0.3441 (9)	6.68
C(2)	0.741 (1)	0.4772 (9)	0.4670 (8)	2.67	O(2)	0.303 (2)	0.762 (2)	0.659 (2)	6.44
C(3)	0.894 (1)	0.2524 (9)	0.5107 (8)	2.93					
				$[Au_2(dmpe)_2]I_2 \cdot CH_3CN$					
Au(1)	0.60853 (7)	0.07439 (3)	−0.40714 (4)	0.80	C(8)	0.881 (2)	0.1152 (8)	−0.302 (1)	iso
Au(2)	0.49107 (7)	0.08112 (3)	−0.28129 (3)	0.80	C(9)	0.830 (2)	0.0008 (7)	−0.2985 (9)	iso
Au(3)	0.80900 (7)	0.18409 (3)	−0.02536 (4)	0.82	C(10)	0.768 (2)	0.0023 (7)	−0.2342 (8)	iso
Au(4)	0.99284 (7)	0.11339 (3)	0.05653 (4)	0.80	C(11)	0.572 (2)	−0.0023 (7)	−0.1490 (9)	iso
I(1)	0.6585 (1)	0.15227 (5)	−0.16263 (6)	1.38	C(12)	0.535 (2)	−0.0604 (7)	−0.2757 (9)	iso
I(2)	1.2723 (1)	0.15269 (5)	0.13049 (6)	1.30	C(13)	0.925 (2)	0.2715 (7)	−0.1326 (9)	iso
I(3)	0.2109 (1)	0.02728 (5)	−0.23788 (6)	1.36	C(14)	1.099 (2)	0.2562 (7)	−0.0150 (9)	iso
I(4)	0.7227 (1)	0.17626 (5)	−0.48257 (7)	1.53	C(15)	1.072 (2)	0.1764 (7)	−0.1175 (8)	iso
P(1)	0.4073 (5)	0.0811 (2)	−0.4641 (2)	0.78	C(16)	1.160 (2)	0.1343 (7)	−0.0773 (9)	iso
P(2)	0.3900 (5)	0.1588 (2)	−0.3167 (2)	0.83	C(17)	0.967 (2)	0.0529 (8)	−0.1024 (9)	iso
P(3)	0.8109 (5)	0.0587 (2)	−0.3541 (2)	0.99	C(18)	1.209 (2)	0.0325 (8)	−0.0212 (9)	iso
P(4)	0.5913 (5)	0.0053 (2)	−0.2385 (2)	0.83	C(19)	0.577 (2)	0.0890 (7)	0.0163 (9)	iso
P(5)	0.9796 (5)	0.2211 (2)	−0.0707 (2)	1.04	C(20)	0.492 (2)	0.1979 (8)	−0.007 (1)	iso
P(6)	1.0786 (5)	0.0826 (2)	−0.0353 (2)	0.84	C(21)	0.645 (2)	0.1714 (7)	0.1164 (8)	iso
P(7)	0.6337 (5)	0.1594 (2)	0.0258 (2)	0.97	C(22)	0.742 (2)	0.1362 (7)	0.1598 (9)	iso
P(8)	0.9114 (5)	0.1454 (2)	0.1497 (2)	0.99	C(23)	0.990 (2)	0.1169 (7)	0.2260 (9)	iso
C(1)	0.287 (2)	0.0299 (7)	−0.4437 (9)	iso	C(24)	0.936 (2)	0.2174 (7)	0.1599 (9)	iso
C(2)	0.410 (2)	0.0768 (7)	−0.5531 (8)	iso	N(1)	−0.060 (2)	−0.0953 (8)	−0.4280 (9)	iso
C(3)	0.324 (2)	0.1448 (7)	−0.4565 (8)	iso	C(25)	0.046 (2)	−0.0907 (9)	−0.406 (1)	iso
C(4)	0.270 (2)	0.1554 (8)	−0.3904 (9)	iso	C(26)	0.179 (2)	−0.0874 (8)	−0.3757 (9)	iso
C(5)	0.493 (2)	0.2130 (7)	−0.3342 (9)	iso	N(2)	0.281 (2)	0.2985 (9)	−0.141 (1)	iso
C(6)	0.294 (2)	0.1853 (7)	−0.2556 (9)	iso	C(27)	0.387 (2)	0.3007 (9)	−0.149 (1)	iso
C(7)	0.934 (2)	0.0452 (7)	−0.4092 (9)	iso	C(28)	0.522 (2)	0.3030 (9)	−0.172 (1)	iso

[a] $B(\text{eqv}) = {}^4/_3[a^2b(11) + b^2b(22) + c^2b(33) + ab(\cos\gamma)b(12) + ac(\cos\beta)b(13) + bc(\cos\alpha)b(23)]$. [b] Primed atoms are disordered with 50% occupancy each. [c] See Experimental Section for explanation of disorder.

Table III. Comparison of the Structural Features of the Crystallographically Characterized $[Au_2(dmpm)_2]^{2+}$ and $[Au_2(dmpe)_2]^{2+}$ Cations

compd	Au···Au, Å	Au–P, Å	P–Au–P, deg	twist, deg[a]
$[Au_2(dmpm)_2](ClO_4)_2$	3.028 (2)	2.313 (5)	178.0 (3)	
$[Au_2(dmpm)_2]Cl_2\cdot 2H_2O$[b]	3.010 (1)	2.300 (2)	176.61 (5)	
$[Au_2(dmpm)_2]Br_2\cdot 2H_2O$	3.023 (1)	2.304 (2)	176.7 (1)	
$[Au_2(dmpe)_2](ClO_4)_2\cdot H_2O$	2.872 (2)	2.285 (4)	174.7 (2)	51
$[Au_2(dmpe)_2]Cl_2\cdot 2H_2O$	2.9265 (5)	2.293 (6)	178.1 (1)	55
$[Au_2(dmpe)_2]Br_2\cdot 1.5H_2O$	2.9438 (5)	2.297 (9)	177.4 (9)	54
$[Au_2(dmpe)_2]I_2\cdot CH_3CN$	2.974 (3)	2.293 (7)	175 (3)	51

[a] The twist of the P–Au–P fragments in the $[Au_2(dmpe)_2]^{2+}$ cations is defined as the average of the acute P–Au–Au*–P* torsion angles. [b] Reference 4.

Table IV. Anion···Au Contacts (Å)

	$[Au_2(dmpm)_2](ClO_4)_2$		
Au···O(1)[a,b]	3.32 (8)	Au···O(3)[a,c]	3.35 (4)
Au···O(2)′[a,b]	3.70 (6)		
	$[Au_2(dmpm)_2]Br_2\cdot 2H_2O$		
Au···Br	3.537 (2)	Au···Br[d]	3.494 (2)
	$[Au_2(dmpe)_2](ClO_4)_2\cdot H_2O$		
Au···O(2)[e,f]	3.58 (3)		
	$[Au_2(dmpe)_2]Cl_2\cdot 2H_2O$		
Au(1)···Cl(1)	3.028 (6)	Au(2)···Cl(2)	3.0218 (5)
	$[Au_2(dmpe)_2]Br_2\cdot 1.5H_2O$		
Au(1)···Br(1)	3.111 (1)	Au(2)···Br(2)	3.0830 (4)
	$[Au_2(dmpe)_2]I_2\cdot CH_3CN$		
Au(1)···I(4)	3.267 (1)	Au(2)···I(1)	3.331 (1)
Au(2)···I(3)	3.425 (1)	Au(3)···I(1)	3.151 (1)
Au(4)···I(2)	3.277 (1)		

[a] Atoms are related to those in Table II by $x, y, 1 + z$. [b] $1 - x, 1 - y, 1 - z$. [c] $1 - x, y, 1 - z$. [d] $1 - x, 1 - y, 2 - z$. [e] $-x - 1, -y, z$. [f] $-y, -x - 1, -z - 2$.

(1) and 2.304 (2) Å average for the bromide. As shown in Table III, these values compare well with those for the previously determined Cl^- salt.[4]

In each salt the anions are centered above the plane of the cations. The bromide is ordered with two Au···Br^- contacts, which average 3.52 (2) Å (Table IV), and two hydrogen bonds. The Au···Cl^- contacts average 3.49 (2) Å in the previously determined Cl^- salt.[4] The perchlorate anion is disordered and presents two different faces toward the cation plane: three oxygen atoms in one orientation, two in the other. As a result, the chlorine atoms are fractionally disordered, the molecule presenting three oxygen atoms toward the cation plane exhibiting the closer Cl approach. This latter anion also exhibits the closest Au···O contacts, which average 3.34 (2) Å versus 3.70 (6) Å for O(2)′, the closest approach of the other anion orientation.

Structures of the $[Au_2(dmpe)_2]^{2+}$ Salts. Each cation in the four determinations has approximately the same overall geometry. Unlike those in the dmpm analogues, the linear P–Au–P units are twisted relative to one another by an average of 53 (1)°. A view of the twist in the cation of the bromide salt is presented in Figure 2.

The different packing environments in the four salts discussed below may be responsible for the observed differences in Au···Au distances, which range from 2.872 (2) Å in the perchlorate salt to 2.974 (3) Å in the iodide salt. The range in Au···Au separations, 0.1 Å, is much larger than the observed range in average Au–P bond distance (2.285 (4) Å (ClO_4^-) to 2.297 (9) Å (Br^-)). The iodide, for which the longest Au···Au distance was observed, was the only one of these four salts to be studied at low temperature.

The immediate environments of the gold atoms in the four determinations are quite different. In the perchlorate salt, the anions reside on either side of the Au···Au vector, the closest Au···O contact being 3.58 (3) Å. The unique water molecule has all of its close contacts with the perchlorate anion.

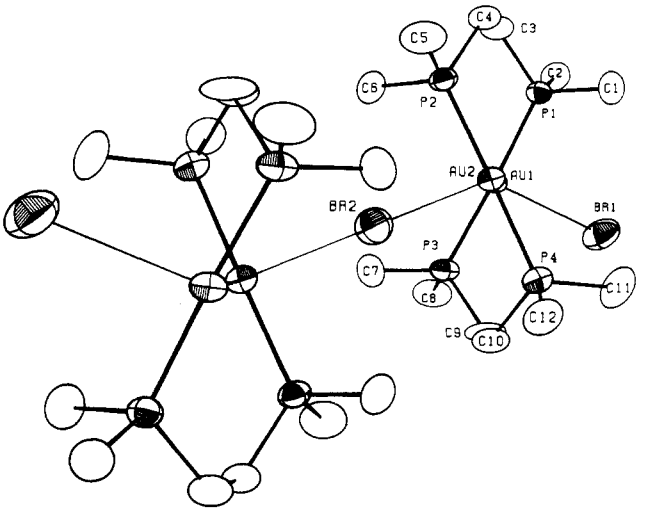

Figure 2. View of $[Au_2(dmpe)_2]Br_2\cdot 1.5H_2O$ down the Au–Au vector.

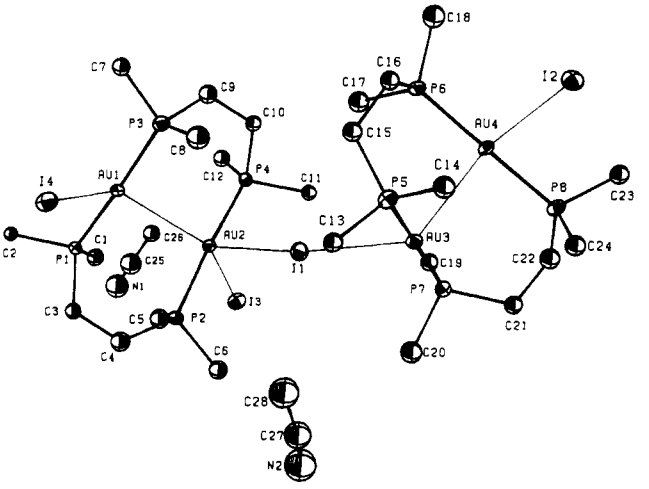

Figure 3. Asymmetric unit of $[Au_2(dmpe)_2]I_2\cdot CH_3CN$.

Each Au atom in the isostructural chloride and bromide salts has one close contact with a halide ion. X(2) resides on a center of inversion and has two such contacts just over 3.0 Å. X(1) has one Au···X contact (also just over 3.0 Å) and accepts two hydrogen bonds. The third unique anion is disordered across a center of inversion and accepts three (Br^-) or four (Cl^-) hydrogen bonds. Taken together, these contacts form polymeric chains of anion/water molecules/cation/anion/cation/anion/water molecules.... The Au(1)···Br(1) and Au(2)···Br(2) contacts are only slightly longer, 3.111 (1) and 3.0830 (4) Å, respectively, than the Au···Cl separations of 3.028 (6) and 3.0218 (5) Å, and both are much longer than observed Au–X covalent bonds.[22]

The asymmetric unit for $[Au_2(dmpe)_2]I_2\cdot CH_3CN$ is depicted in Figure 3. As in the chloride and bromide salts, each gold atom has at least one close anion contact; however, in this structure Au(2) has two such contacts. I(1) is centered between Au(2) and Au(3) (as X(2) was for the other two halide structures) slightly closer to Au(3), for which this is the only anion contact. I(3) is the second anion contact for Au(2) and along with I(2) and I(4) has only one cation close contact. The acetonitrile molecules separate the units associated around I(1).

Absorption and MCD Spectra for the Perchlorate Salts. Figures 4 and 5 present absorption and MCD spectra for $[Au_2(dmpm)_2](ClO_4)_2$ and $[Au_2(dmpe)_2](ClO_4)_2$, respectively, in 0.08 M $HClO_4$. Quantitative spectral data for both $HClO_4$ and CH_3CN solvents are collected in Table V, where data for the mononuclear $[Au(PEt_3)_2]PF_6$ complex in CH_3CN[23] are included

(22) Braunstein, P.; Mueller, A.; Boegge, H. *Inorg. Chem.* **1986**, *25*, 2104.

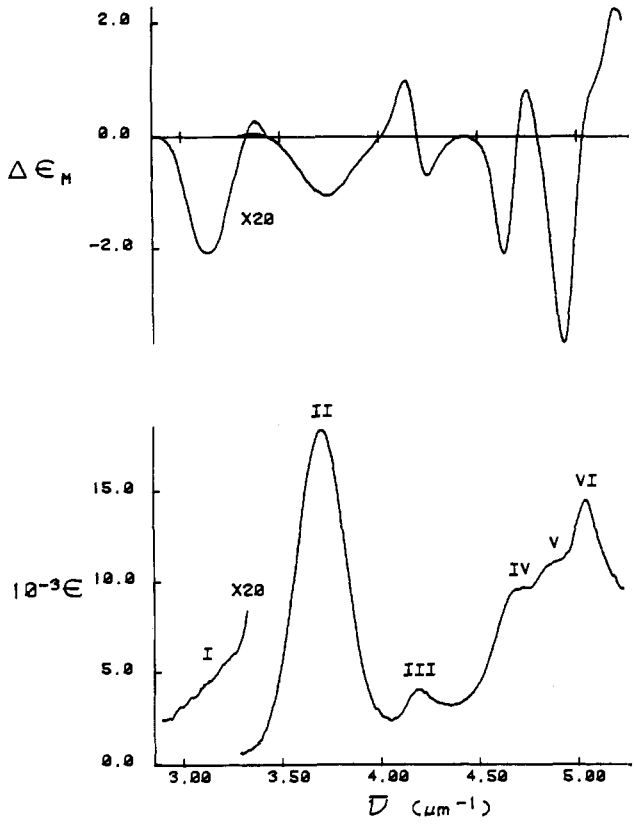

Figure 4. Electronic absorption (lower curves) and MCD (upper curves) spectra for $[Au_2(dmpm)_2](ClO_4)_2$ in 0.08 M $HClO_4$. The data in the range 2.8–3.3 μm^{-1} were each multiplied by a factor of 20 before plotting.

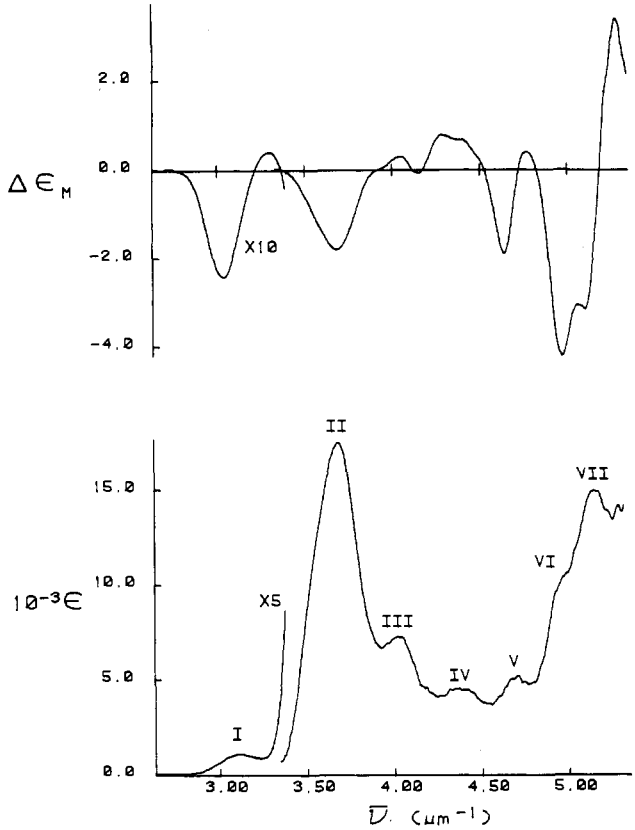

Figure 5. Electronic absorption (lower curves) and MCD (upper curves) spectra for $[Au_2(dmpe)_2](ClO_4)_2$ in 0.08 M $HClO_4$. The absorption and MCD data in the range 2.7–3.3 μm^{-1} were multiplied by factors of 5 and 10, respectively, before plotting.

for comparison. The absorption spectra for the perchlorate salts in dilute $HClO_4$ compare favorably with the spectra reported for

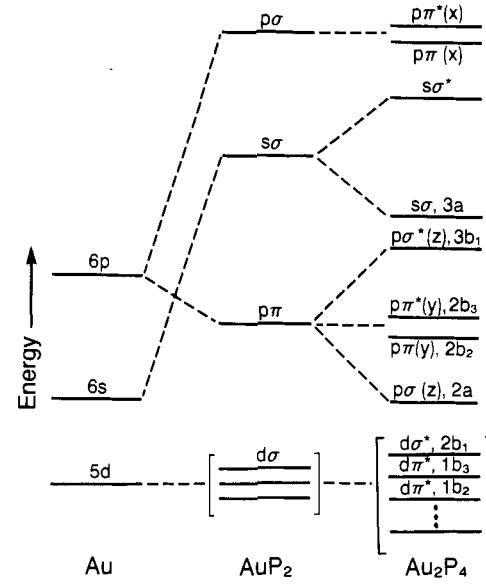

Figure 6. Schematic molecular orbital energy level diagram for the mononuclear AuP_2 and the binuclear Au_2P_4 complexes (the z axis is along the Au–Au vector and the x axis is parallel to the AuP_2 units or bisects them).

the chloride salts in water.[5] In each case the binuclear complex shows two bands (I and II) and their associated MCD features at energies lower than and with intensities different from those of the lowest energy absorption and MCD bands of the mononuclear $[Au(PEt_3)_2]^+$ cation[23] (Table V). The red shift of the lowest energy bands for the binuclear Au_2P_4 complexes compared to those for the related AuP_2 complex is logically ascribed to intramolecular Au–Au interaction in the d^{10}–d^{10} complexes. However, a detailed description of the transitions and an interpretation of the MCD spectra require a careful consideration of the electronic states for the binuclear complexes.

Electronic States and MCD Terms. Figure 6 presents a schematic MO energy-level diagram for the Au_2P_4 binuclear complexes together with levels for the mononuclear AuP_2 complex for comparison. The local symmetry of the Au_2P_4 cluster (P-methyls and bridging carbon(s) neglected at a first approximation) is D_{2h} for the dmpm complex (parallel linear AuP_2 units) and D_2 for the dmpe complex (AuP_2 units twisted 53° about the Au–Au vector away from parallel). For most of the present analysis D_2 symmetry is sufficient, since D_{2h} is simply D_2 plus inversion. The coordinate origin is placed midway between the Au atoms, the Au–Au vector is taken to be the z axis, and the x axis lies parallel to the AuP_2 units or bisects them, respectively, in the dmpm or dmpe complex. Thus, the Au orbitals directed along z are expected to be the most strongly affected by the Au–Au interaction. In particular, bonding and antibonding combinations of $5d_{z^2}$ (filled), 6s, and $6p_z$ are visualized as giving rise to Au_2-localized orbitals labeled $d\sigma^*$, $s\sigma$, $p\sigma$, etc. in Figure 6. This consideration leads to the reasonable conclusion that the $d\sigma^*$ combination of the filled $5d_{z^2}$ orbitals, $2b_1$, in Figure 6, is most likely the highest energy occupied orbital (HOMO) for these d^{10}–d^{10} binuclear complexes. The $d\pi^*$ combinations of $5d_{xz}$ and $5d_{yz}$, $1b_2$ and $1b_3$, respectively, are expected to be the next highest energy filled MO's. The ground states for the Au_2P_4 complexes are therefore $...(1b_2)^2(1b_3)^2(2b_1)^2$, diamagnetic and totally symmetric (^1A). The lowest energy unoccupied orbitals (LUMO's) are visualized similarly: the combinations of empty 6s and $6p_z$ are the most strongly affected by the close approach of the two Au atoms. The relative energies of the empty orbitals for AuP_2 are based on our previous study of the linear $[Au(PEt_3)_2]^+$ ion.[23] Table VI lists the lowest energy excited configurations, the zero-order singlet and triplet states for these configurations in the absence of spin–orbit coupling, and the spin–orbit states that result from strong gold spin–orbit

(23) Savas, M. M.; Mason, W. R. *Inorg. Chem.* **1987**, *26*, 301.

Table V. Spectral Data

band no.	absorption $\bar{\nu}$, μm^{-1}	absorption λ, nm	absorption ϵ, $(M\ cm)^{-1}$	MCD $\bar{\nu}$, μm^{-1}	MCD $\Delta\epsilon_M$, $(M\ cm\ T)^{-1}$	band no.	absorption $\bar{\nu}$, μm^{-1}	absorption λ, nm	absorption ϵ, $(M\ cm)^{-1}$	MCD $\bar{\nu}$, μm^{-1}	MCD $\Delta\epsilon_M$, $(M\ cm\ T)^{-1}$
					$[Au_2(dmpm)_2](ClO_4)_2$ in 0.080 M $HClO_4$						
I	3.13	319	200[a]	3.13	−0.10	IV	4.70	213	9800		
				3.35	+0.065					4.75	+0.84
II	3.72	269	18400	3.73	−1.06	V	4.86	206	11100		
				4.14	+1.00					4.93	−3.68
III	4.20	238	4170			VI	5.04	198	14600		
				4.24	−0.70					5.11	+1.14[a]
				4.64	−2.08					5.20	+2.23
					$[Au_2(dmpm)_2](ClO_4)_2$ in CH_3CN						
I	3.13	320	500[a]	3.13	−0.23	IV	4.66	215	13200		
II	3.69	271	25500	3.73	−1.43					4.74	+1.08
				4.11	+0.96	V	4.89	204	13400		
III	4.17	240	6550							4.94	−5.02
				4.22	−0.89	VI	5.05	198	19100		
				4.47	+0.34					5.10	+1.03[a]
				4.63	−2.45					5.20	+3.29
					$[Au_2(dmpe)_2](ClO_4)_2$ in 0.080 M $HClO_4$						
I	3.11	321	230	3.03	−0.24	V	4.70	213	5200		
				3.29	+0.044					4.77	+0.41
II	3.68	272	17600	3.68	−1.80	VI	4.97	201	10200[a]	4.97	−4.2
III	4.03	248	7400	4.05	+0.31					5.10	−3.16
				4.15	−0.08	VII	5.14	195	15000		
				4.28	+0.81					5.27	+3.39
IV	4.37	229	4300								
				4.40	+0.69[a]						
				4.64	−1.89						
					$[Au_2(dmpe)_2](ClO_4)_2$ in CH_3CN						
I	3.06	327	900	3.03	−0.29	V	4.67	214	7000		
II	3.67	273	21800	3.65	−1.75					4.76	+0.79
III	4.02	249	10500	4.04	+0.34	VI	4.91	204	10900[a]	4.96	−4.06
				4.15	−0.06					5.09	−3.11
				4.31	+0.83	VII	5.13	195	17400		
IV	4.36	229	7200							5.27	+2.75
				4.63	−1.44						
					$[Au(PEt_3)_2](PF_6)$ in CH_3CN[b]						
I	3.98	251	1150	3.97	−1.49	III	4.78	209	14000		
				4.06	+0.31					4.81	−6.04
				4.16	+0.52	IV	4.88	205	15500	4.87	0
II	4.20	238	1740							4.93	+2.90
				4.24	−0.26	V	5.08	197	14200[a]	5.09	−0.48[a]
				4.33	+0.50					5.20	−4.17[a]
				4.68	−2.45	VI	5.22	192	12000	5.23	−4.84
					$Au_2(dmpm)_2^{2+}$ + Cl^- in CH_3CN[d,e]						
				3.02	(−0.10)[a]	II	4.12	243	21000	3.99	(−0.72)
I	3.40	294	7400	3.50	(−0.26)[a]					4.21	(−0.41)[a]
				3.75	(−0.32)[a]						
					$Au_2(dmpm)_2^{2+}$ + Br^- in CH_3CN[d,f]						
I	3.40	294	5500[a]			II	3.93	254	25000	4.00	(+0.05)
				3.82	(−1.09)					4.12	(−0.15)
					$Au_2(dmpe)_2^{2+}$ + Cl^- in CH_3CN[d,g]						
I	3.20	313	7500	3.24	(−0.25)	II	4.08	245	18000	3.96	(−0.16)
				3.66	(−0.12)[a]					4.19	(−0.16)
					$Au_2(dmpe)_2^{2+}$ + Br^- in CH_3CN[d,h]						
I	3.04	329	8300	3.10	(−0.30)	II	4.00	250	27000	4.00	(−0.44)[a]
				3.47	(−0.10)[a]						
					$Au_2(dmpe)_2^{2+}$ + I^- in CH_3CN[d,i]						
I	2.80	357	8000	2.81	(−0.24)	II	3.75	267	32000	3.73	(−0.82)

[a] Shoulder. [b] Data from ref 23. [c] *A* term. [d] Numbers in parentheses for MCD spectra are $10^3\Delta A$ values at 7.0-T field and 1.00-cm path for the concentrations specified in footnotes *e–i*. [e] $[Au_2^{2+}] = 6.6 \times 10^{-5}$ M, $[Cl^-] = 9.7 \times 10^{-4}$ M. [f] $[Au_2^{2+}] = 6.7 \times 10^{-5}$ M; $[Br^-] = 6.9 \times 10^{-5}$ M. [g] $[Au_2^{2+}] = 6.1 \times 10^{-5}$ M; $[Cl^-] = 1.22 \times 10^{-3}$ M. [h] $[Au_2^{2+}] = 6.1 \times 10^{-5}$ M; $[Br^-] = 5.6 \times 10^{-4}$ M. [i] $[Au_2^{2+}] = 6.4 \times 10^{-5}$ M; $[I^-] = 9.2 \times 10^{-5}$ M.

coupling ($\zeta_{5d} \sim 0.5\ \mu m^{-1}$) within the zero-order states. Allowed electronic transitions are permitted to the B_1, B_2, and B_3 spin–orbit states (*z*, *y*, and *x* polarized, respectively). The transitions to states of spin-forbidden triplet parentage can gain significant intensity by intermixing with states of singlet origin that have the same symmetry and arise from configurations that differ by no more than one spin orbital. All of the excited states of the binuclear complexes are nondegenerate due to the D_2 (or D_{2h}) symmetry. Therefore, the MCD spectrum will consist entirely of *B* terms, which arise through magnetic interaction between nondegenerate states in the presence of the external field. Derivative type MCD *A* terms, which arise from Zeeman splitting of degenerate states,

Table VI. Excited Configurations and States

excited confgn[a]	zero-order states[b]	spin–orbit states[b,c]	parity[d]
$(2b_1)(2a)$	$^1B_1$	B_1	u
	$^3B_1$	(A), B_3, B_2	u
$(2b_1)(2b_2)$	$^1B_3$	B_3	g
	$^3B_3$	B_2, B_1, (A)	g
$(2b_1)(2b_3)$	$^1B_2$	B_2	u
	$^3B_2$	B_3, (A), B_1	u
$(1b_3)(2a)$	$^1B_3'$	B_3'	g
	$^3B_3'$	B_2', B_1', (A′)	g
$(1b_3)(2b_2)$	$^1B_1'$	B_1'	u
	$^3B_1'$	(A′), B_3', B_2'	u
$(1b_3)(2b_3)$	$^1A'$	(A′)	g
	$^3A'$	B_1', B_2', B_3'	g
$(1b_2)(2a)$	$^1B_2''$	B_2''	g
	$^3B_2''$	B_3'', (A″), B_1''	g
$(1b_2)(2b_2)$	$^1A''$	(A″)	u
	$^3A''$	B_1'', B_2'', B_3''	u
$(1b_2)(2b_3)$	$^1B_1''$	B_1''	g
	$^3B_1''$	(A″), B_3'', B_2''	g

[a] Filled orbitals omitted. [b] Prime and double-prime notation indicates excitation from different filled orbitals. [c] Forbidden A symmetry states in parentheses. [d] Parity subscripts for D_{2h} symmetry.

will be absent, although two close-lying states (energy difference less than their transition bandwidths) that interact in the field will give B terms of opposite sign and therefore can give the appearance of an A term (pseudo-A term).[14] MCD C terms, of course, will be zero because the ground states are diamagnetic.

A number of possible excited configurations and states were considered in order to interpret the MCD B terms in the measured spectra, including several that are expected to be higher in energy than those listed in Table VI. However, only a few were found to give both nonzero electric and magnetic moment matrix elements, which are necessary for MCD B terms. The allowed cases are limited to the interaction between certain B_1 and B_2 excited states. For the space-averaged case the B terms are given by $\bar{B}_0$ parameters in eq 3[14] for an $A \rightarrow B_1(j)$ transition, where μ_B = Bohr

$$\bar{B}_0(B_1(j),B_2(k)) = \frac{-2}{3\mu_B}\left[\sum\frac{1}{\Delta W_{kj}}\langle B_1(j)||\mu^{B_2}||B_2(k)\rangle \times \langle A||\mathbf{m}^{B_1}||B_1(j)\rangle\langle B_2(k)||\mathbf{m}^{B_2}||A\rangle\right] \quad (3)$$

magneton, $\mu = \mu_B(\mathbf{L} + 2\mathbf{S})$, $\mathbf{m} = e\mathbf{r}$, the magnetic moment and electric dipole operators, and $\Delta W_{kj} = W_k - W_j$, the energy difference between the states k and j. The value of B_0 for an $A \rightarrow B_2(k)$ transition is $-\bar{B}_0(B_1(j),B_2(k))$.[14] The spin–orbit states from the configurations involving $d\sigma^*$, $2b_1$ (unprimed states of Table VI), are given in eq 4 and 5; similar equations can be written for

$$|B_1(j)\rangle = a_j|^1B\rangle + b_j|^3B_2\rangle + c_j|^3B_3\rangle \quad (4)$$

$$|B_2(k)\rangle = d_k|^1B_2\rangle + e_k|^3B_1\rangle + f_k|^3B_3\rangle \quad (5)$$

the orthogonal $d\pi^*$ configurations involving $1b_3$ and $1b_2$ (primed and double primed states of Table VI). When eq 4 and 5 are substituted into eq 3, eq 6 results when the one-electron MO's

$$\bar{B}_0(B_1(j),B_2(k)) = \frac{-2}{3\mu_B}\left[\sum\frac{1}{\Delta W_{kj}}(a_j^*d_k(-\mu_B/\sqrt{2}) + b_j^*e_k(-\mu_B/\sqrt{2}) + c_j^*f_k(-2\mu_B))a_jd_k^*M_0M_1\right] \quad (6)$$

are approximated by pure 5d, 6s, and 6p orbitals on the gold atoms. In eq 6 $M_0 = -2\langle 2b_1|m_z^{b_1}|2a\rangle$ and $M_1 = \langle 2b_3|m_y^{b_2}|2b_1\rangle$ are one-electron electric dipole matrix elements and the summation is assumed to include only the states of eq 4 and 5 because contributions from other states are expected to be negligible due to a large ΔW_{kj}. The M_0 and M_1 integrals are difficult to calculate exactly, but their sign can be predicted from overlap considerations on the basis of the coordinate system used and standard conventions[12] (M_0 is negative and M_1 is positive).

Spectral Interpretation. A comparison of the absorption and MCD spectra for the Au_2P_4 cations with spectra for the mononuclear $[Au(PEt_3)_2]^+$ cation (Table V) shows two distinct regions: a low energy region (bands I and II for the Au_2P_4 complexes) below the lowest energy band (at 3.98 μm^{-1}) for $[Au(PEt_3)_2]^+$ and a higher energy region (bands III–VI or –VII for the dmpm or dmpe complex), where $[Au(PEt_3)_2]^+$ also displays several bands. The appearance of bands I and II for the Au_2P_4 cations to the red side of the lowest energy band in the spectra for $[Au(PEt_3)_2]^+$ strongly suggests the Au–Au-localized $d\sigma^* \rightarrow p\sigma$ transitions for the binuclear complexes. Figure 6 shows that the $p\sigma$ LUMO for the Au_2P_4 complexes is stabilized through Au–Au interaction relative to the $p\pi$ LUMO of the AuP_2 complex (the $d\sigma^*$ HOMO for Au_2P_4 is also expected to be destabilized relative to the filled d orbitals of AuP_2), which leads to a red shift for the lowest energy transitions for Au_2P_4 compared to those for AuP_2. On the other hand, the absorption bands and their associated MCD features for the binuclear complexes in the higher energy region are similar to those observed for the mononuclear $[Au(PEt_3)_2]^+$ cation (bands II–VI), which were previously assigned as $d \rightarrow p\pi$ transitions of Figure 6 (a combination of metal to ligand charge transfer (MLCT) and 5d → 6p Au transitions).[23] This similarity provides strong support for interpreting the spectra for the binuclear complexes in the high-energy region in terms of several AuP_2-localized transitions.

Bands I and II for the Au_2P_4 cations can be satisfactorily interpreted in terms of transitions to states of the $d\sigma^* \rightarrow p\sigma$ $(2b_1)(2a)$ lowest energy excited configuration (Figure 6, Table VI). The orbitals of this configuration are primarily Au_2 localized, which is supported by the striking similarity of both absorption and MCD spectra in the region of bands I and II for the dmpe complex compared to those for the dmpm complex. Specifically, the MCD spectra for both complexes exhibit negative B terms for bands I and II in both dilute $HClO_4$ and CH_3CN solvents and a weak positive B term between them in dilute $HClO_4$, which is unresolved in CH_3CN solution. Consideration of eq 6 leads to the conclusion that transitions to B_1 or B_2 states that interact with higher energy B_2 or B_1 states, respectively, will give rise to negative B terms (negative $\bar{B}_0$ parameters). Therefore band I, which appears as a weak shoulder near 3.1 μm^{-1} for the dmpm complex but is better resolved for the dmpe complex, is assigned as the transition to the spin–orbit state $B_2(^3B_1)$ of the $(2b_1)(2a)$ configuration. The negative B term is predicted by eq 6 primarily from interaction of this state with $B_1(^3B_2)$ $[(2b_1)(2b_3)]$, which lies at higher energy. The low intensity of band I is consistent with the triplet parentage of the $B_2(^3B_1)$ state. The intense band II at 3.7 μm^{-1} for both complexes is assigned as the transition to $B_1(^1B_1)$ $[(2b_1)(2a)]$, the lowest energy predominantly singlet state. The observed negative B term can be traced primarily to an interaction with the higher energy $B_2(^1B_2)$ $[(2b_1)(2b_3)]$ state. It may be remarked here that predictions of B-term sign for transitions to states of intermediate energy, such as $B_1(^1B_1)$, that can potentially interact with other states both at higher and lower energy (the $B_2(^3B_1)$ state) is sometimes problematic unless the precise location of all interacting states is known. However, for the $B_1(^1B_1)$ state just discussed there is no interaction with the lower energy $B_2(^3B_1)$ state to first order because both states involve the same orbital functions but different spin functions. The interaction of the $B_1(^1B_1)$ state with the only other B_2 state to higher energy, $B_2(^3B_3)$ $[(2b_1)(2b_2)]$, is expected to be small because of the low singlet character in the latter (the interaction is also parity-forbidden in D_{2h}). Therefore, there is little ambiguity in the B-term-sign predictions for bands I and II from eq 6. Finally, the weak positive B term observed in the MCD spectra between bands I and II in dilute $HClO_4$ signals the presence of another weak transition. This transition may be to $B_3(^3B_1)$ $[(2b_1)(2a)]$, which is expected at energy near that for $B_2(^3B_1)$ but which is expected to be weak in both absorption and MCD because the electric dipole of the transition to the $B_3(^1B_3)$ $[(2b_1)(2b_2)]$ state

from which it derives intensity is very small (zero in a D_{2h} one-center approximation).

The similarity of the absorption and MCD spectra for the Au_2P_4 cations to the spectra of $[Au(PEt_3)_2]^+$ in the high-energy region can be explained by noting the placement of the nearly degenerate $p\pi(y)$ and $p\pi^*(y)$ Au_2P_4 orbitals compared to the degenerate $p\pi$ AuP_2 orbital in Figure 6. Excitation from the filled 5d orbitals will produce several excited states at similar energies for both complexes. Therefore, a mapping of the $d \rightarrow p\pi$ AuP_2 states[23] to $d \rightarrow p\pi(y)$, $p\pi^*(y)$ Au_2P_4 states should serve as a useful guide by which to interpret the spectra of the binuclear complexes. For example, the intense bands III and IV for $[Au(PEt_3)_2]^+$ (Table V) were assigned as $d \rightarrow p\pi$ transitions to predominantly singlet spin–orbit states a,b $^1\Pi$, while the weaker bands I and II were interpreted as transitions to the corresponding a,b $^3\Pi$ spin–orbit states (see ref 23 for details). For the Au_2P_4 cations, the $B_2(^1B_2)$ $[(2b_1)(2b_3)]$ and $B_1'(^1B_1')$ $[(1b_3)(2b_2)]$ states would be analogous to a,b $^1\Pi$, while $B_1(^3B_2)$ $[(2b_1)(2b_3)]$, $B_2'(^3B_1')$ $[(1b_3)(2b_2)]$, and $B_1''(^3A'')$, $B_2''(^3A'')$ $[(1b_2)(2b_2)]$ will correspond to the a,b $^3\Pi$ spin–orbit states. Therefore, on the basis of energy and intensity, bands V and VI for the dmpm complex and bands VI and VII for the dmpe complex are assigned to transitions to the states of singlet origin $B_1'(^1B_1')$ and $B_2(^1B_2)$, respectively. The positive *B* term associated with the latter is expected from eq 6 through interaction with the lower energy $B_2(^1B_2)$ state responsible for band II discussed above. The negative *B* term for the $B_1'(^1B_1')$ state is not as easy to predict but would not be unreasonable on the basis our analysis similar to eq 6 involving an interaction with a higher energy B_2 state beyond the range of our measurements. The MCD spectrum near 5.1 μm^{-1} also exhibits a weaker feature between the strong negative and positive terms associated with the $B_1'(^1B_1')$ and $B_2(^1B_2)$ states. A specific assignment of this feature is not possible, but a number of weaker $d \rightarrow p\pi(y)$, $p\pi^*(y)$ transitions are expected in this region.

The weaker bands in the 4.0–4.8-μm^{-1} region (III–V for the dmpe complex and III and IV for the dmpm complex) show some dependence on the ligand between the two Au_2P_4 complexes but are logically assigned as $d \rightarrow p\pi(y)$, $p\pi^*(y)$ transitions to the spin–orbit states of triplet origin in both cases. Specific assignments in this region are rendered difficult owing to the high density of states possible for the Au_2P_4 complexes and the complexity of the spectra. For example, the dmpe complex exhibits three distinct bands compared to two for the dmpm complex, with corresponding differences in the MCD spectra. These differences are likely due to small changes in relative energy of some of the states present in this region. Thus, it is possible to imagine bands IV and V of the dmpe complex being combined into one unresolved band IV for the dmpm complex if the state(s) associated with the dmpe band IV were to shift slightly to higher energy. Further, the MCD spectrum in the region of band III for the dmpm complex has the appearance of a negative pseudo *A* term at 4.2 μm^{-1} and therefore indicates at least two unresolved transitions with associated *B* terms of opposite sign. The transition to $B_1(^3B_2)$ $[(2b_1)(2b_3)]$ is suggested for the positive *B* term at 4.1 μm^{-1}, which is predicted by eq 6 through interaction with the low-energy $B_2(^3B_1)$ state (band I, negative *B* term) discussed above. The assignment of the positive *B* term for band III of the dmpe complex would be analogous. The assignments of the other features in the 4.2–4.8-μm^{-1} region are less clear, but certainly transitions to $B_2'(^3B_1')$ $[(1b_3)(2b_2)]$ and $B_1''(^3A'')$, $B_2''(^3A'')$ $[(1b_2)(2b_2)]$ are anticipated to be the strongest.

Spectral Studies for CH_3CN Solutions Containing Halide. The absorption spectra for the halide salts of the $Au_2P_4^{2+}$ cations in water or dilute $HClO_4$ were essentially the same as for the perchlorate salts (Figures 4 and 5), except for the halide counterion absorptions. However, in CH_3CN the spectra for the halide salts were notably different and Beer's law was not obeyed. Figure 7 presents absorption and MCD spectra for $Au_2(dmpe)_2^{2+}$ with excess halide in CH_3CN; Figure 8 shows spectra for $Au_2(dmpe)_2^{2+}$ and $Au_2(dmpm)_2^{2+}$ with excess chloride. Since Beer's law does not hold, the concentrations of $Au_2P_4^{2+}$ and halide are specified in the figure captions. The changes in these spectra as a function

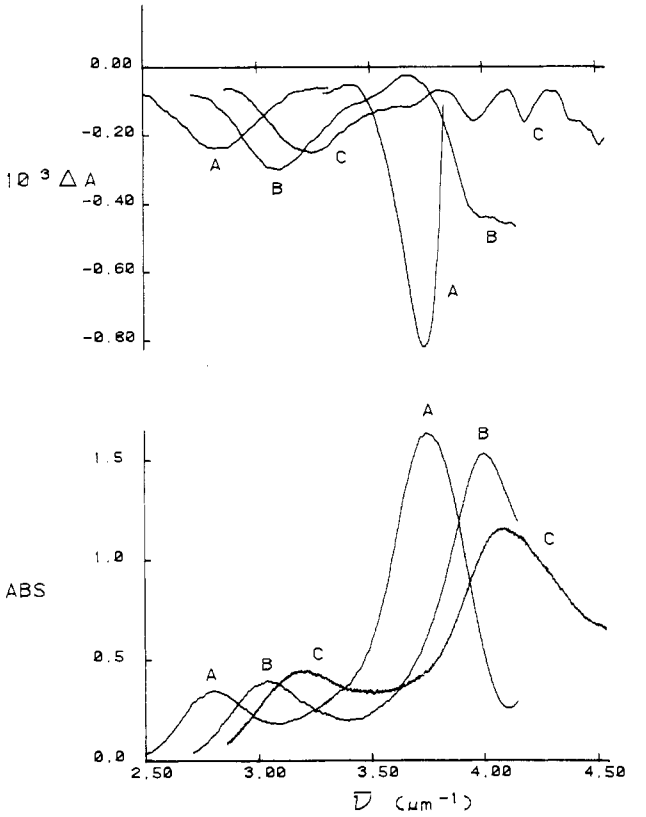

Figure 7. Electronic absorption (lower curves) and MCD (upper curves) spectra in CH_3CN for $Au_2(dmpe)_2X^+$ ($Au_2(dmpe)_2^{2+} + X^-$): (A) $[I^-] = 9.2 \times 10^{-5}$ M, $[Au_2^{2+}] = 6.4 \times 10^{-5}$ M; (B) $[Br^-] = 5.6 \times 10^{-4}$ M, $[Au_2^{2+}] = 6.1 \times 10^{-5}$ M; (C) $[Cl^-] = 1.22 \times 10^{-3}$ M, $[Au_2^{2+}] = 6.1 \times 10^{-5}$ M. The MCD spectrum A in the range 2.5–3.3 μm^{-1} was multiplied by a factor of 3 before plotting. All spectra were obtained at 7.0-T field with a 1.00-cm path.

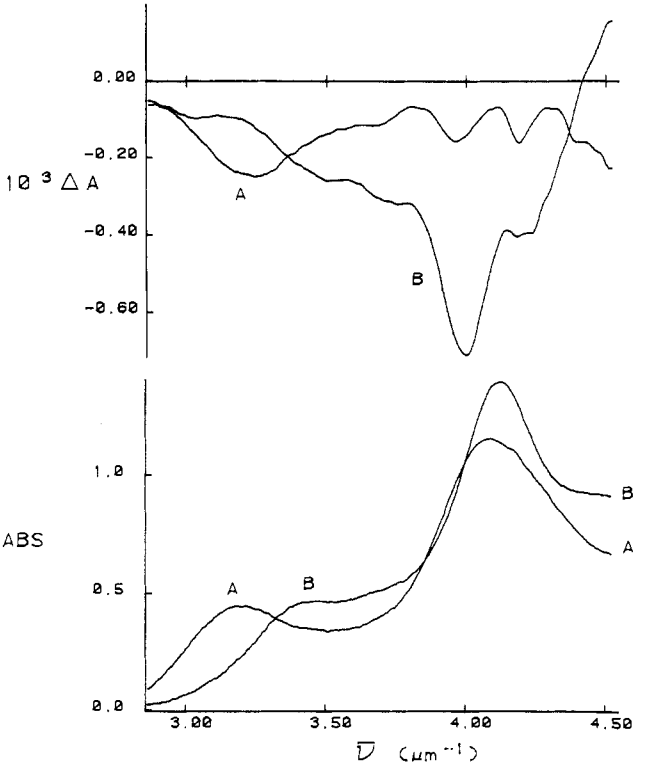

Figure 8. Electronic absorption (lower curves) and MCD (upper curves) spectra in CH_3CN for $Au_2P_4Cl^+$ ($Au_2P_4^{2+} + Cl^-$): (A) dmpe, $[Au_2^{2+}] = 6.1 \times 10^{-5}$ M, $[Cl^-] = 1.22 \times 10^{-3}$ M; (B) dmpm, $[Au_2^{2+}] = 6.6 \times 10^{-5}$ M, $[Cl^-] = 9.2 \times 10^{-4}$ M. All spectra were obtained at 7.0-T field with a 1.00-cm path.

Table VII. Association Constants in CH_3CN at 22 °C

cation	halide	$10^{-4}K$, M^{-1} [a]	cation	halide	$10^{-4}K$, M^{-1} [a]
$[Au_2(dmpe)_2]^{2+}$	Cl^-	1.5 (2)	$[Au_2(dmpm)_2]^{2+}$	Cl^-	4.4 (3)
$[Au_2(dmpe)_2]^{2+}$	Br^-	5.4 (7)	$[Au_2(dmpm)_2]^{2+}$	Br^-	22 (2)
$[Au_2(dmpe)_2]^{2+}$	I^-	8.1 (4)			

[a] Standard deviation in parentheses.

of cation and halide concentration are consistent with an association equilibrium to form $Au_2P_4X^+$ (eq 1). Quantitative studies permitted the evaluation of association constants by using eq 2; values of these constants are summarized in Table VII. Band positions and approximate molar absorptivities for $Au_2P_4X^+$ were determined from solutions of $Au_2P_4^{2+}$ in equilibrium with excess X^-, subtracting absorption contributions due to the small amounts of unassociated cation and the absorption due the X^- ion and then normalizing to the equilibrium concentration of Au_4X^+. These spectral data are included in Table V. The MCD data in Table V for CH_3CN solutions containing excess halide were corrected for halide MCD data by subtracting blank solutions containing the halide alone (CH_3CN solutions of halide, especially I^-, have significant MCD signals above 4.0 μm^{-1}, which have been attributed to charge transfer to solvent (CTTS) transitions[24]). The MCD intensity data in Table V are given as ΔA values for the field and concentration conditions specified.

The association equilibrium to form $Au_2P_4X^+$ in CH_3CN and the lack of significant association in aqueous solution is understandable in view of the lower dielectric constant for CH_3CN than for water and the tendency for the $Au_2P_4^{2+}$ cations to interact strongly with halides in the solids investigated here. The association constants (Table VII) are halide dependent, though not strongly so, with the order $I^- > Br^- > Cl^-$, which is typical of halide interaction with soft metal ions such as Au(I). The constants also show that the dmpm complex is more strongly associated in CH_3CN than the dmpe complex with the same halide, but the effect is less than a factor of 5 and may reflect differences in solvation or steric considerations between the two types of complexes.

The marked difference between the spectra of the associated $Au_2P_4X^+$ species and the unassociated $Au_2P_4^{2+}$ cations is interesting. The spectra in Figure 7 show that the band positions are halide dependent, and Figure 8 shows that there is also some dependence on the cation. The halide dependence with band energies $I^- < Br^- < Cl^-$ is consistent with $X^- \rightarrow$ Au ligand to metal charge transfer (LMCT) in the associated complex. Since the LUMO for $Au_2P_4^{2+}$ is pσ, the transitions can be visualized as $X^-\pi \rightarrow$ pσ (band I) and $X^-\sigma \rightarrow$ pσ (band II). The relative intensity of the two band systems together with the energy separation of 0.7–1.0 μm^{-1} is typical for LMCT in halide complexes.[25] The observation that the $X^-\sigma \rightarrow$ pσ transition occurs at an energy higher than that of the intense d$\sigma^* \rightarrow$ pσ transition of the unassociated cation suggests that there is some halide covalent bonding to the pσ orbital and therefore some halide character in this orbital in the $Au_2P_4X^+$ complex. An alternative assignment of band II for the $Au_2P_4X^+$ complexes to a blue-shifted d$\sigma^* \rightarrow$ pσ transition as a result of the halide interaction with pσ is also a possible interpretation, but the MCD spectra show differences between band II for $Au_2P_4X^+$ and $Au_2P_4^{2+}$, with the MCD spectrum for $Au_2P_4X^+$ being more complicated. Finally, the dependence of the spectra on the cation may reflect some small changes in relative stability of the pσ LUMO resulting from differences in $X^- \rightarrow Au_2^{2+}$ donation and Au charge in the $Au_2P_4X^+$ complex. The energy of band I is the most strongly affected, with the order dmpm > dmpe. This is the same order as that for the association constants and may reflect stronger $X^- \rightarrow Au_2^{2+}$ bonding, but as noted above, the differences are rather small.

Concluding Remarks. It is clear from both the Au–Au distances in the solids and the position of the lowest energy spectral bands of $Au_2P_4^{2+}$ at an energy lower than that of the related AuP_2^+ complex that the interaction between the Au centers is important. This interaction has been attributed to relativistic effects primarily involving the 6s orbital on Au.[26] The mixing of 6s, and to a lesser extent $6p_z$, with the dσ and dσ^* orbitals of $Au_2P_4^{2+}$ will serve to provide a significant bonding interaction in the ground state and is responsible for the short Au–Au distance in the annular cations. The relativistic aspect of the interaction is further illustrated when $Au_2(dmpm)_2^{2+}$ is compared with the silver analogue of the same molecular structure. The Ag–Ag distance (3.041 (2) Å) in $[Ag_2(dmpm)_2](PF_6)_2$[27] is actually *longer* for the smaller Ag atoms and thus reflects lower relativistic effects in the 5s orbital of Ag compared to the 6s orbital of Au.[26] Finally, it is noteworthy that the energy of the intense d$\sigma^* \rightarrow$ pσ transition in the solution spectra is practically the same for $Au_2(dmpm)_2^{2+}$ and $Au_2(dmpe)_2^{2+}$, even though there is a significant difference between the Au–Au distances in the solid perchlorate salts. The d$\sigma^* \rightarrow$ pσ transition energy is expected to be a sensitive function of the Au–Au interaction, and therefore this result suggests that the Au–Au distance in the two $Au_2P_4^{2+}$ cations in solution is not appreciably different. The difference in Au–Au distances in the solids must be due to crystal packing.

Acknowledgment is made to the donors of the Petroleum Research Fund, administered by the American Chemical Society, for support of this work and to the NSF Chemical Instrumentation Program for funds used to purchase the diffractometer.

Supplementary Material Available: Tables SI–SXXI, listing crystal data, thermal parameters, derived hydrogen positions, and bond distances and angles, and Figures A–G, showing ORTEP views of $[Au_2(dmpm)_2](ClO_4)_2$ and cell packing diagrams of each compound studied (29 pages); tables of calculated and observed structure factors (59 pages). Ordering information is given on any current masthead page.

(24) El-Kourashy, A.-G.; Grinter, R. *J. Chem. Soc., Faraday Trans. 2* **1977**, *73*, 1050.
(25) Blanchard, W. D.; Mason, W. R. *Inorg. Chim. Acta* **1978**, *28*, 159.
(26) Pyykkö, P. *Chem. Rev.* **1988**, *88*, 563.
(27) Karsch, H. H.; Schubert, U. *Z. Naturforsch.* **1982**, *37b*, 186.